Research Article Vol. 14, No. 2 / 1 Feb 2023 / Biomedical Optics Express 639
Biomedical Optics EXPRESS

Optical memory effect of excised cataractous human crystalline lenses

ALBA M. PANIAGUA-DIAZ,[1,*] DULCE M. SIMÓN,[1] CARMEN MARTÍNEZ,[1] ELENA MORENO,[1] ALBA RODRÍGUEZ-RÓDENAS,[1] INÉS YAGO,[2] JOSE MARÍA MARÍN,[2] AND PABLO ARTAL[1]

[1]*Laboratorio de Óptica, Universidad de Murcia, Campus de Espinardo, 30100 Murcia, Spain*
[2]*Oftalmología, Hospital Universitario "Virgen de la Arrixaca", El Palmar, Murcia, Spain*
[*]*a.paniagua-diaz@um.es*

Abstract: Cataracts increase the amount of scattered light in the crystalline lens producing low-contrast retinal images and causing vision impairment. The Optical Memory Effect is a wave correlation of coherent fields, which can enable imaging through scattering media. In this work, we characterize the scattering properties of excised human crystalline lenses by measuring their optical memory effect and other objective scattering parameters, finding the relationship between them. This work has the potential to help fundus imaging techniques through cataracts as well as the non-invasive correction of vision through cataracts.

1. Introduction

Cataracts is a common ocular pathology that increases scattering in the crystalline lens causing blur and reduced contrast in the retinal images [1,2]. Most cataracts are related to the aging process, although these can also be developed because of injuries, high exposure to UV light, or other eye diseases [3]. The opacifications of the crystalline lens in the eye are caused by protein aggregation within the lens, which scatters light in all directions. This prevents existing imaging techniques to successfully image the fundus of the eye, despite the diagnostic interest that it has before cataract surgery. Even a high-quality cataract surgery can have disappointing results if there are unknown pre-existing retinal pathologies, such as age-related macular degeneration or diabetic retinopathy among others [4,5].

Thanks to the deterministic nature of the scattering process [6,7], different approaches are being suggested to allow imaging through scattering media to a certain degree [8–11]. Several emerging imaging techniques in scattering media are based on exploiting the intrinsic correlations of the transmitted light, as the Optical Memory Effect (OME) [12–14]. The OME depends on the scattering properties and scattering strength of the medium under study, and it provides information of their isoplanatic patch [15].

Currently the only solution to cataracts is surgery, where the eye's crystalline lens is removed and substituted by an artificial intraocular lens. In a recent work, a possible alternative was suggested based on the optical correction of scattering by using wavefront shaping techniques [16]. An improvement of the eye's PSF was obtained in a cataract's eye model, achieving a promising improvement in the simulated optimized retinal images, assuming isoplanatism in the full image extension. However, this ideal isoplanatism is not realistic in all cases, but it will depend on the Optical Memory Effect of the cataractous lens.

The OME has been extensively studied in highly isotropic scattering materials with a thin slab geometry (in the order of few micrometers) and very large optical densities, being well characterized in these terms [15]. Schott *et al.* extended the study to characterize the OME to biological media, where the scattering anisotropy is relevant [17]. They found the expected OME range was surprisingly increased in the case of anisotropic scattering, which allowed them

#480678 https://doi.org/10.1364/BOE.480678
Journal © 2023 Received 10 Nov 2022; revised 18 Dec 2022; accepted 23 Dec 2022; published 5 Jan 2023

Biomedical Optics EXPRESS

to measure it in relatively thick slabs (reaching about 1 mm), although a rigorous theoretical explanation to it is still missing [15,17].

Here we characterize the scattering properties and OME of excised human crystalline lenses with different grades of cataracts. These results could be useful for the design of appropriate imaging approaches through the lenses based on transmission correlations and wavefront shaping techniques.

2. Methods

In this study we measured a total of 16 different lenses from donors aged between 29 and 61 years old, at different cataract stages, with a total of 34 different measurements. Most of the lenses were received clear. Cataracts were developed in the excised crystalline lenses by leaving the lenses immerse in Eusol-c (Alchimia Srl) for several weeks. Eusol-c is a synthetic liquid for corneal storage and conservation, which also helps the lens to slow deterioration, making the cataract formation process more controllable. The different measurements were taken during a period of approximately 5 months, where some lenses were tested several times, at different cataract stages.

2.1. Qualitative scattering characterization

2.1.1. Point Spread Functions

The Point Spread Function (PSF) describes the response of an optical imaging system to a point source. We recorded the PSF of the different crystalline lenses using the experimental setup of Fig. 1. A 594 nm laser beam (5 mW 05-LYR-173, Melles Griot, Carlsbad, California, USA) is expanded by lenses L1 and L2 to a diameter of 5 mm impinging on the crystalline lens, immersed in a cuvette (CV10Q14F, Thorlabs Inc., Germany) with Eusol-c. A second 4-f telescope formed by lenses L3 and L4 form the image of the PSF into a CMOS camera (DCC1545M; Thorlabs Inc., Germany). The axial position of the camera was shifted in each case to obtain the sharpest focus, to adjust for the power of each of the lenses. All the images were taken with different exposure times of the camera, maximizing the signal but avoiding saturation, in order to use the maximal dynamic range of the camera.

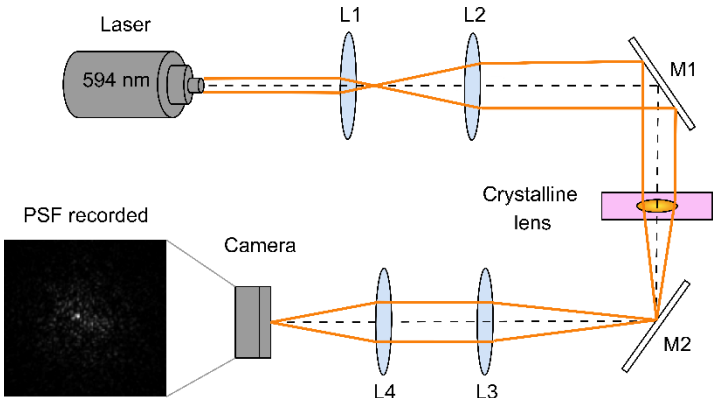

Fig. 1. Schematic of the setup for the measurement of the PSF of the crystalline lenses.

2.1.2. Dark field photography

Dark field images of the crystalline lenses were recorded to qualitatively evaluate their opacities. Figure 2 (a) shows the schematic of the custom-built apparatus for the acquisition of the dark

Biomedical Optics EXPRESS

field images. Light from a ring of white LEDs passes through a central hole covered by a glass slide, on top of which the crystalline lens is placed, immerse in the cuvette with Eusol-c. Due to the off-axis illumination, only the scattered light is imaged and acquired by the CMOS camera (UI-324xCP-NIR, IDS Imaging Development Systems GmbH, Germany). The parameters of the camera (i.e., gain and exposure time), as well as the illumination power of the LEDs were fixed for the acquisition of all tested lenses, allowing a direct comparison among them. Figure 2(b) shows an example of a crystalline lens, where the whitish areas correspond to the ones generating more scattering. Fig. 2(c) shows an image of USAF-target formed through the lens.

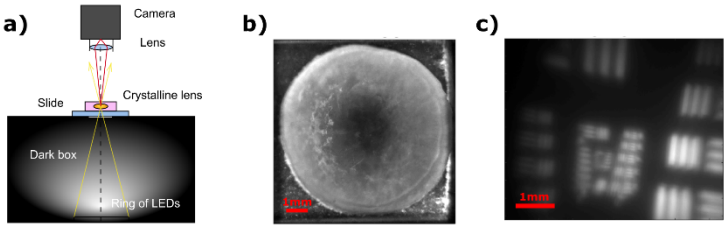

Fig. 2. (a) Setup for the dark field photography. Only the scattered light is captured by the camera. (b) Dark Field Image of a crystalline lens with a mature cataract. (c) USAF-target image through lens shown in (b) with a Michelson Contrast of 0.64.

2.2. Objective scattering characterization

2.2.1. Optical Integration Method

The Optical Integration Method is a technique based on the projection of monochromatic disks onto the retina, in order to measure the intraocular straylight.

The term straylight refers to the intraocular scattered light. We usually classify this scattered light as backward or forward scattering, depending on its propagation direction. Traditionally, backward straylight is used to evaluate both objectively and/or subjectively the intraocular scattering, for instance using the slit-lamp images and the LOCS III classification and reference images [18]. However, the backward straylight does not only involve the light reflected back from the opacities in the lens, but it also includes the light reflected from the fundus and transmitted by the lens. It is the forward straylight, reaching the retina, the one that causes vision impairment by blurring and reducing the contrast of retinal images. In this way, forward scattering is a more useful quantity to determine the impact of cataracts and its vision impairment capabilities [19,20]. Indication for cataract surgery based on the straylight values have been suggested in the literature [20]. In this work we are interested in the characterization of the straylight parameter because of its clinical relevance, since it is possible to measure it in patients in vivo, as it has been already demonstrated [19].

The angular dependence of the lens straylight (s) is given by the product between the point spread function (PSF) and the angle (θ) squared [21]:

$$s(\theta) = \theta^2 PSF(\theta). \tag{1}$$

The PSF of the studied lenses as function of θ was measured using the optical integration method [22]. This technique is based on the projection of monochromatic disks with varying diameter (2θ) and uniform irradiance through the crystalline lenses whilst recording the central intensity ($I_c(\theta)$) of their images. I_c is the summation of the weighted contributions PSF(φ) from

Biomedical Optics EXPRESS

all the bright sources at a radial distance φ within the disk:

$$I_c(\theta) = \int_0^{\theta} 2\pi\varphi PSF(\varphi)d\varphi. \tag{2}$$

Once $I_c(\theta)$ is normalized to its maximum value, PSF(θ) is given by:

$$PSF(\theta) = \frac{1}{2\pi\theta}\frac{dI_c(\theta)}{d\theta}. \tag{3}$$

Figure 3 shows the experimental setup for the optical integration method. The disks were displayed with a FHD LCoS screen (Syndiant 2281, Syndiant Inc., USA) illuminated with a Xenon lamp (Model E7536, Hamamatsu, Japan). A telescope composed of lenses L1 and L2 conjugates the entrance pupil with the crystalline lens plane, immersed in the cuvette with Eusol-c. The illumination diameter on the lens is 5 mm. A spectral filter (FB550-40; Thorlabs Inc., Germany) was placed $s(\theta) = \theta^2 PSF(\theta)$ before L1 to produce a quasi-monochromatic illumination with central wavelength 550 ± 8 nm.

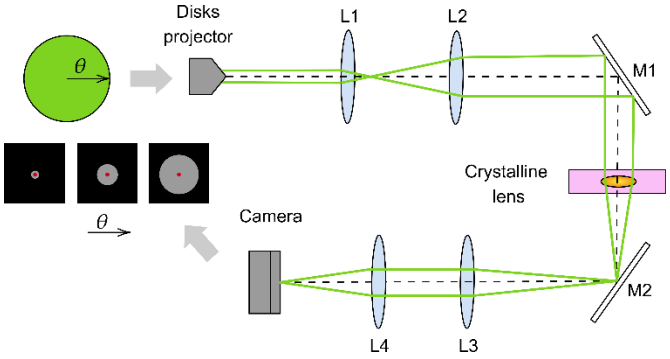

Fig. 3. Schematic of the Optical Integration Method system, for the measurement of the straylight as function of θ in the different lenses. Green ray tracing depicts the light trajectory when the lens is tested. The focusing for each lens is manually adjusted by the axial displacement of the camera.

For each crystalline lens, disks were imaged on a CMOS camera (DCC1545M; Thorlabs Inc., Germany) by the 4-f telescope formed by lenses L3 and L4. Since the different crystalline lenses had different power, the camera was axially displaced to adjust the focus in each case. The amount of straylight provided by the optical system (or the baseline) was measured when the cuvette was with Eusol-c and a clear auxiliary lens, which was directly subtracted from the measurements.

For the calculation of the straylight, several disks with sizes of 2θ were displayed and the central intensity of their images (the position marked by the red dot in Fig. 3 was recorded. The angular distribution of the PSF is then calculated from the angular local slopes of the central intensities, according to Eq. (3). For each straylight measurement, 114 disks were projected, where the processed central intensity corresponds to the mean of three sequential measurements. The dark noise of the camera and the effects of parasitic light were also taken into account by subtracting the intensity (at the center of the disks) when no image was displayed on the projector.

Figure 3 shows examples of the acquired disks and the central intensity as function of θ. The local angular slopes of the central intensity were computed to calculate the PSF following Eq. (3). The maximal angular range of the measured PSF is 6.1°. It is mainly determined by the size of the display projecting the disks and the focal length of the collimating lens. The PSFs retrieved with Eq. (3) are normalized on the solid angle of 25.9×10^{-3} steradian (sr). The units of the PSF and s are sr^{-1} and $deg^2 sr^{-1}$, respectively, although the logarithmic values of the straylight

Biomedical Optics EXPRESS

(Log_{10}(s)) are used to compare with other approaches [19]. From the whole angular range, we use the values at 3 degrees as reference for off-axis straylight intensity, with which we compare the rest of measurements.

2.2.2. Image contrast

Using the set-up of Fig. 3, we also recorded images through each of the lenses, when displaying an USAF-test target in the LCoS display (instead of the solid disks described before). The Michelson contrast of the images was quantified. Some examples can be found in Fig. 2(c) and Fig. 5(d-f). All the images were taken with different exposure times of the camera, maximizing the signal but avoiding saturation, in order to use the whole camera's dynamic range. A second image with the same exposure time and a blank display was subsequently taken for a posterior subtraction, accounting for the effects of parasitic light or camera dark noise.

2.3. Optical Memory Effect

The Optical Memory Effect (OME) is a well-known wave correlation observed in coherent fields, which allows the control and information retrieval of scattered light from diffuse media [12–15]. It describes an intrinsic isoplanatism of the scattering medium for small angles and displacements even in strong scattering media, where small tilts or shifts of the incident wavefront with respect to the medium generates speckle patterns that do not decorrelate immediately but hold correlations between them, dependent on the scattering properties of the medium. A speckle pattern is an apparently random interference pattern of light when emerging from a scattering medium, as shown in the inset of Fig. 4.

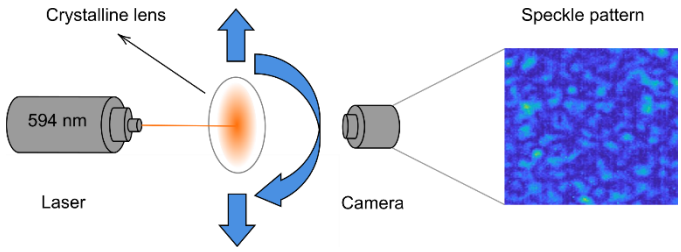

Fig. 4. Schematic of the experimental configuration for the measurement of the shift and tilt optical memory effect. A laser beam at 594 nm wavelength impinges onto a crystalline lens mounted in a translation and rotation stage, after which a CCD camera is placed to record the transmitted speckle patterns.

In our case, this gives us an approximation of the isoplanatic patch of the correction imaging technique described in [16], determining how the transmitted speckle pattern from cataractous lenses change with a tilt/shift of the incident beam. We measured this effect using a 2 mm diameter laser beam at 594 nm wavelength, incident on the cataractous lenses and recording the transmitted speckle pattern at each position. With the lens mounted on a shift/tilt optomechanical holder, we moved the position of the lens with respect to the static beam for simplicity. The similarity between the speckle patterns for different values of shift or tilt of the lens were examined via a normalized cross-correlation.

First, a static set of measurements consisting of 10 images was taken, spaced 1 minute between them, to test the temporal decorrelation of the system. In all cases the temporal decorrelation was completely negligible in ten minutes, barely reaching a 1% decorrelation. This ensures that in the rest of the tests, taking less than ten minutes each, we were capturing mainly the decorrelation due to tilt or shift of the lens respect to the incident beam, no static temporal decorrelation artifacts.

Biomedical Optics EXPRESS

Figure 4 shows a simplified schematic of the experimental setup. A laser of 594 nm (5 mW 05-LYR-173, Melles Griot, Carlsbad, California, USA) is incident on a cuvette with the lens, mounted on a combined translation stage and a goniometer, allowing us to have control over the linear translation (shift) and angular rotation of the sample (tilt). The sample was moved whereas the illumination part remained unchanged. The center of rotation of the goniometer was coincident with the position of the sampled lens. The camera was placed at 12.5 cm from the lens, farther from its focal length, of about 5 cm. Although the ideal situation would have been to take the images at the focal plane, the size of the speckle spots made it difficult, so we placed the camera farther in order to have larger-size speckle spots. We tested the OME range for one lens at two distances, one very close to the focal plane where each speckle spot cover between 1 and 2 pixels and the other with the camera farther away, with the speckle spots being around 4 pixels wide, with no significant changes in the OME range but reduced noise. In general, being farther than its focal spot means that the OME measured might be slightly smaller than the real one, although no big changes are expected.

3. Results

Figure 5 shows examples of the measured crystalline lenses, presenting different levels of opacities corresponding to straylight parameters of 1,76, 1,99 and 2,47 at 3 degrees for panels (a)-(c), respectively. The image of a target formed through each of these lenses (using the experimental setup shown in Fig. 3) is shown in panels (d)-(f) of the same figure. The Michelson contrast of the images are 0,89 for panel (d), 0,64 in panel (e) and 0,08 for panel (f). Each column corresponds to measurements performed with the same lens. Panels (g)-(i) represent the corresponding PSF associated to each lens. As the lenses become opaquer, the PSF spreads, associated with a more diffuse corresponding image. The extension of the PSF images correspond to areas of 1mm^2.

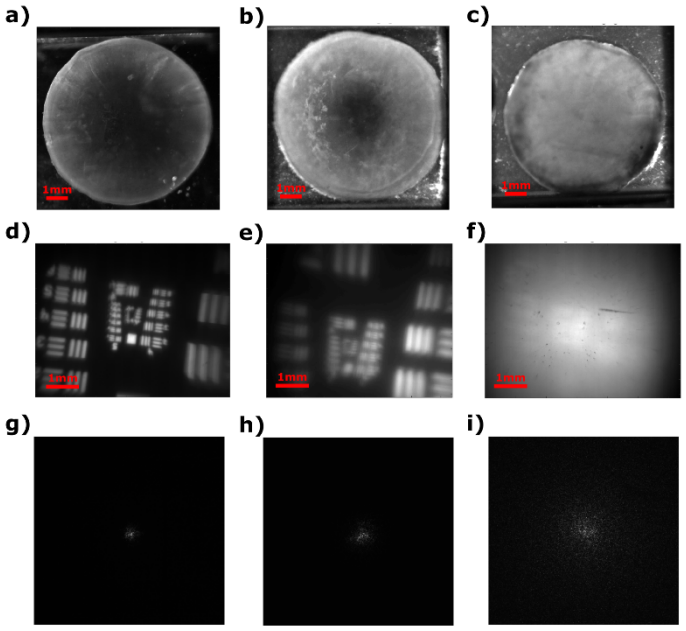

Fig. 5. (a)-(c) Dark Field Images of crystalline lenses with straylight parameters at 3 degrees of 1,76, 1,99 and 2,47, respectively. (d)-(f) Images of an USAF test target through the tested lenses shown in panels (a)-(c), respectively. (g)-(i) PSF of the corresponding lenses in the same columns. The image corresponds to an area of 1mm^2.

Biomedical Optics EXPRESS

In Fig. 6(a),(b) we show examples of the shift and tilt OME measurements for different straylight values ($Log_{10}(s)$) or scattering strength. We took two different measurements, the first one shifting (or laterally translating) the sample in one direction, in steps of 20 µm, reaching up to 400 µm in displacement. An image of the transmitted speckle pattern was taken for every step and with a posterior post-processing we obtained the normalized cross-correlation as a function of displacement. As seen in Fig. 6(a), the decorrelation curves are also different for the different straylight values, decaying more exponentially as the scattering strength (or straylight value) increases. The second part of this measurement consisted on tilting (or rotating) the lens with respect to the illumination beam, in controlled steps of 10 arcmin and 30 arcmin, reaching a total of 1.4 degrees with 0.17 degrees resolution and 5.5 degrees with 0.5 degrees resolution, only in one direction. As in the previous case, a post-processing of the set of measurements gave the normalized cross-correlation as function of the rotation angle, as seen in Fig. 6(b). We can also observe the exponential trend as the straylight increases. Due to the symmetric nature of cataract formation, as can be observed from Fig. 5(a)-(c), a symmetric behavior is expected, so we only performed the measurements in one direction for time efficiency. In Fig. 6(c)-(f), we represent the obtained relationship between the straylight parameter at 3 degrees and the rest of parameters measured for each lens. Fig. 6(c) shows the linear relationship between the straylight parameter and the Michelson contrast of the images taken through the lenses. As expected, the larger the straylight parameter, i.e. the cataract opacity, the smaller the contrast of the images. This clear linear trend, with an $R^2 = 0.81$, provides us with a solid confirmation that the straylight parameter at 3 degrees is a rigorous way of quantifying lens scattering. The empirical formula relating the straylight of crystalline lenses and the contrast of their transmitted images is given by:

$$C = -0.7 \cdot Log_{10}(s)|_{3^\circ} + 2 \tag{4}$$

where $Log_{10}(s)|_{3^\circ}$ is the straylight parameter at 3 degrees. In Fig. 6(d) we represent the decorrelation obtained for a tilt of 1 degree in each of the lenses, again with respect to their straylight parameter. As we can observe from the graph, they are related by a linear trend with an $R^2 = 0.74$. The larger the value of straylight of the lenses, the faster the transmitted speckle patterns decorrelate when the lens is tilted 1 degree with respect to the reference, ranging from the almost negligible decorrelation for straylight parameters around 1.3 deg^2sr^{-1}, to the almost complete decorrelation for values around 2.6 deg^2sr^{-1}. This relation is given by:

$$OME_{Tilt(1^\circ)} = -0.7 \cdot Log_{10}(s)|_{3^\circ} + 2. \tag{5}$$

In a similar fashion, in the graph of Fig. 6(e) we plot the straylight parameter vs the normalized decorrelation for a lateral shift of 400 µm. From the linear trend, holding an $R^2 = 0.69$, we can observe again how for more opaque lenses (higher straylight parameter) the speckle patterns decorrelate faster, reaching the 400 µm displacement completely decorrelated, in contrast to the more transparent ones, where at that distance the speckle patterns are barely decorrelated. The experimental relationship obtained between the shift decorrelation at 400 µm and the straylight parameter is:

$$OME_{Shift(400\mu m)} = -0.5 \cdot Log_{10}(s)|_{3^\circ} + 1.5. \tag{6}$$

Figure 6(f) provides us with an easier interpretation of the isoplanatism of cataractous lenses. There we plot the values of the straylight of the lenses versus the angle at which the decorrelation decays to half of its normalized value. It can be considered that two speckle patterns are decorrelated when the normalized cross-correlation is smaller than 0.5, or half its normalized value. In the graph we also find a linear trend relating the straylight of the lenses at 3 degrees with the angular tilt at which the transmitted speckle patterns become decorrelated. This information provides us with half isoplanatic patch of each of the lenses as function of their scattering strength (since we only tilt in one direction). As we can observe from the graph, for the weak scattering

Biomedical Optics EXPRESS

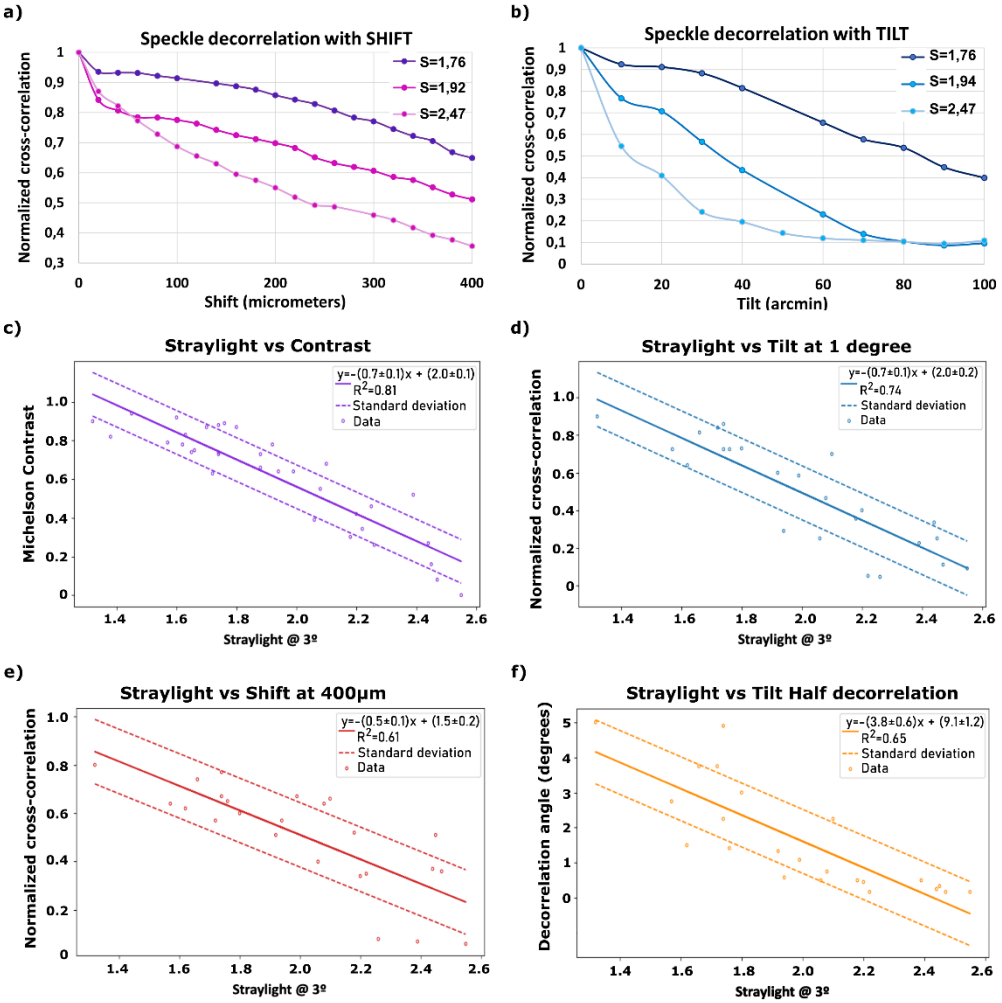

Fig. 6. (a) Normalized cross-correlation of the transmitted speckle patterns for different values of lateral translation, in steps of 20 micrometers. The different curves represent three different crystalline lenses of different opacities, with Straylight parameters ($Log_{10}(s)$) at 3 degrees of 1,76, 1,92 and 2,47, from quasi transparent to opaque. (b) Normalized cross-correlation of the transmitted speckle patterns for different values of tilt or rotation, in steps of 10 arcmin, for the different lenses. (c) Graph showing the relationship between the Michelson contrast of the images and the straylight parameter at 3 degrees. (d) Representation of the normalized cross-correlation for a tilt of 1 degree vs the straylight parameter at 3 degrees of the different lenses. (e) Graph representing the normalized cross-correlation for a shift of 400 um vs the straylight parameter at 3 degrees of the different lenses. (f) In this graph we represent the angles at which the transmitted speckle patterns are decorrelated by half as a function of the straylight of the cataractous lenses, which provides the isoplanatic patch of the media. All the dashed lines represent the standard deviation of the data.

lenses, or early cataracts, the maximal isoplanatic patch is around 5 degrees in one direction (i.e. 10 degrees in total), whereas for the opaquest ones this isoplanatic patch is essentially zero. This empirical relationship can be expressed as:

$$IP = 2 \cdot (-3.8 \cdot Log_{10}(s)|_{3^\circ} + 9) \tag{7}$$

Biomedical Optics EXPRESS

where IP is the Isoplanatic Patch and the factor 2 accounts for the symmetric or total isoplanatic patch, which is two times the decorrelation angle.

In Table 1 we represent the list of the total 34 measurements in lenses, age of the donor, the time the lens has been excised and all relevant measurements.

Table 1. Summary of the relevant measurements and parameters of the measured crystalline lenses

Lens #	Donor age (years)	Excised time (M: Months, D: Days)	Contrast	Straylight @ 3°	OME Tilt (1°)	OME Shift (400um)	Angle @ 0.5 decorrelation (°)
12	46	2 M 14 D	0,66	1,88			
16	46	2 M 12 D	0.75	1.66	0.81	0.74	3.75
16	46	4 M 28 D	0.26	2.26	0.045	0.08	
17	57	27 D	0.87	1.7			
17	57	2 M 3 D	0.46	2.25			
17	57	4 M 25 D	0.52	2.39	0.23	0.07	0.5
18	44	2 M 20 D	0,74	1,74			
18	44	3 M 6 D	0,68	1,62	0,64	0,62	1,5
18	44	5 M 21 D	0,39	2,06	0,25	0,4	0,5
19	44	2 M 9 D	0,79	1,57	0,73	0,64	2,75
19	44	5 M 13 D	0,42	2,2	0,4	0,34	0,45
20	49	2 M 10 D	0,16	2,45	0,25	0,51	0,33
20	49	3 M	0,08	2,47	0,11	0,36	0,17
20	49	4 M 20 D	0	2,55	0,09	0,06	0,17
22	50	15 D	0,83	1,63			
22	50	1 M 27 D	0,64	1,99	0,59	0,67	1,08
22	50	5 M 9 D	0,27	2,44	0,34	0,37	0,25
24	60	1 M 15 D	0,9	1,32	0,9	0,8	5
25	61	3 M 23 D	0,73	1,74	0,73	0,67	2,25
25	61	4 M 14 D	0,68	2,1	0,7	0,66	2,25
26	46	3 M 20 D	0,78	1,92	0,6	0,51	1,33
26	46	4 M 13 D	0,55	2,08	0,47	0,64	0,75
27	56	3 M 19 D	0,64	1,94	0,29	0,57	0,58
27	56	4 M 5 D	0,34	2,22	0,05	0,35	0,17
28	29	5 D	0,94	1,45			
28	29	14 D	0,82	1,38			
28	29	21 D	0,74	1,65			
28	29	1 M 1 D	0,73	1,88			
30	58	20 D	0,92	1,6			
30	58	24 D	0,89	1,76	0,73	0,65	1,4
30	58	1 M 29 D	0,30	2,18	0,36	0,52	0,5
33	48	1 M 18 D	0,87	1,8	0,73	0,6	3
36	42	1 M 15 D	0,88	1,74	0,86	0,77	4,9
37	42	2 M 8 D	0,63	1,72	0,84	0,77	3,75

Biomedical Optics EXPRESS

4. Discussion and conclusions

Cataracts are due to opacifications of the crystalline lens caused by protein aggregations which scatters light in all directions. This has two main consequences, first it produces blurred and low contrast retinal images impairing vision, and second, it prevents existing imaging techniques to image the fundus of the eye or to improve imaging through scattering media. Thanks to the deterministic nature of light scattering, it is possible to use some of its properties, as their Optical Memory Effect, a transmission wave correlation, to unravel the diffuse image or to aid imaging through scattering media [12–14].

In this work we studied cataractous lenses with different degrees of opacity, ranging from early cataracts to mature ones. Due to the nature of cataract formation, even for the same macroscopic scattering parameters, at the microscopic level there will be differences from lens to lens, due to the different position of the scatter centers. However, there are other properties as the scattering-center composition, anisotropy, or scattering attenuation that on average hold minor variations, enabling a rigorous macroscopic comparison. Despite the microscopic scattering variation from lens to lens, we can quantify the macroscopic effect of scattering caused by cataracts in the eye, enabled by the optical integration method measuring the straylight parameter.

The optical integration method used here works in a single-pass through the lens, with the camera placed at the position where the retina would be. However, this method has been already tested in a clinical environment where a double-pass is necessary. To account for the double-pass, this method is based on previous works measuring the double-pass PSF of the eye [23] combined with the projection of disks according to the method of optical integration, which enables the evaluation of straylight up to 8° [22]. This method was performed with green illumination, since it was found that optimal measurements should be done with wavelengths near to the peak of spectral sensitivity of the eye [24]. We also performed a qualitative study of the cataracts, which allowed us to understand better cataract formation. As shown in Fig. 5, we obtained the dark field images highlighting the scattering areas, and how that affected their PSF and image formation. We demonstrated how the dark field images of stronger cataracts (as Fig. 5(c)) corresponded to a broader PSFs (as Fig. 5(i)) and consequently to a blurred and low-contrast image formation through the lenses (as Fig. 5(f)).

The scattering strength of cataracts has been characterized by means of the straylight parameter, using the optical integration method. This method specially interesting since it can be used in clinical practice in patients as non-invasive approach [19]. The scattering strength has been traditionally characterized by the scattering mean free path and anisotropy factor of the medium. In the case of cataracts this is particularly challenging, due to the form factor of the lens and gradient index. There are a few works where these parameters were measured, generally using ultrafast lasers and some of them also slicing the lens into very thin slabs [25–28]. However, although for a physical model these parameters would be of great interest, in the particular case of cataracts a physical model is of limited use, due to the large microscopic variations that we can find in real situations. Moreover, the fact that these metrics cannot be measured in vivo in patients (due to the double-pass configuration of the eye for a non-invasive examination) limits enormously the application of it. For this reason the optical integration method is the preferred approach for categorizing the scattering strength, since it can be used in real patients for clinical applications, which is the final scope of this work.

We characterized the objective straylight parameter of the lenses at several cataract stages, obtaining a direct relationship between them, as well as a linear trend between the degree of scattering or straylight, their image contrast and the maximal range of the OME. We studied the two forms of OME correlation, shift and tilt, although for vision correction tilt is the main measurement of interest due to the nature of image formation, a combination of shift and tilt can be extremely useful for the high-contrast retrieval of fundus images based on the OME [15]. Aided by the strong directionality (or anisotropy) of cataract's scattering, we observed correlations in

Biomedical Optics EXPRESS

relatively thick scattering media, between 3.5 - 4 mm, the average thickness of human crystalline lenses. We also observed different trends in the decorrelation curves (as in Fig. 6(a),(b)), towards an exponential trend for stronger scattering, as observed previously in the literature [17]. The relatively low R^2 of the linear trends might be due to measurement imprecision with the shift and tilt mechanism. Despite the OME is very well described theoretically in a controlled scenario [15], when using that theory for representing this effect in biological media, the model fails to accurately reproduce the experimental results, as it was also found in previous works [15,17].

The knowledge of the OME in cataracts depending on its scattering strength provide us with very valuable information that can be of interest for the visual science community, as it is the isoplanatic patch of the cataract under study. Knowing the isoplanatic patch can be of great importance for imaging techniques based on the OME willing to retrieve high-contrast images hidden behind scattering layers [12,13,15], as it could be the eye's fundus before the cataractous lens is removed, to avoid potential complications during surgery. It can also be essential for the correction of vision through cataracts using non-invasive approaches, as wavefront shaping techniques [16]. Although for the PSF correction it is not necessary, it is important to know over which range the PSF is still optimal, which in the end determines the maximal size of the corrected image, given by the isoplanatic patch of the cataractous lenses. The results obtained represented in Fig. 6 and equations (4)–(7) provide us with a useful tool to predict the decorrelation threshold or the isoplanatic patch of an incident wavefront over cataracts depending on their straylight.

In conclusion, we have characterized and drawn a relationship between different scattering parameters in excised human cataractous lenses, qualitative image measurements and the OME. We have studied the maximal isoplanatic patch allowed by the different lenses depending on their objective straylight parameters, which will be of great help when determining both the optimal approach for fundus imaging through cataracts based on the OME and retinal image correction strategies based on non-invasive wavefront shaping techniques, paving the way for future non-invasive vision correction and fundus imaging through cataracts.

Funding. HORIZON EUROPE Marie Sklodowska-Curie Actions (897300); Agencia Estatal de Investigación (PID2019-105684RB-I00/AEI/10.13039/501100011033).

Acknowledgments. We thank Dr. Jacopo Bertolotti for useful discussions.

Disclosures. The authors declare no conflict of interests.

Data availability. Data underlying the results presented in this paper are available in Ref. [29].

References

1. P. Artal, *Handbook of Visual Optics*, Two-Volume Set. (CRC Press, 2017).
2. D. B. Elliott and M. A. Hurst, "Assessing the effect of cataract: a clinical evaluation of the Opacity Lensmeter 701," Optom. Vis. Sci. **66**(5), 257–263 (1989).
3. P. W. de Waard, J. K. IJspeert, T. J. van den Berg, and P. T. de Jong, "Intraocular light scattering in age-related cataracts," Invest. Ophthalmol. Vis. Sci. **33**(3), 618–625 (1992).
4. B. A. Henderson, J. Y. Kim, C. S. Ament, Z. K. Ferrufino-Ponce, A. Grabowska, and S. L. Cremers, "Clinical pseudophakic cystoid macular edema. Risk factors for development and duration after treatment," J. Cataract Refractive Surg. **33**(9), 1550–1558 (2007).
5. Z. Farhan, *Cataract Surgery*, Chap. 25, (IntechOpen, 2013).
6. E. Akkermans and G. Montambaux, *Mesoscopic physics of electrons and photons* (Cambridge University Press, 2007).
7. J. W. Goodman, *Speckle phenomena in optics: theory and applications* (Roberts & Company Publishers, 2007).
8. I. M. Vellekoop and A. P. Mosk, "Focusing coherent light through opaque strongly scattering media," Opt. Lett. **32**(16), 2309–2311 (2007).
9. S. M. Popoff, G. Lerosey, M. Fink, A. C. Boccara, and S. Gigan, "Controlling light through optical disordered media: transmission matrix approach," New J. Phys. **13**(12), 123021 (2011).
10. J. Kubby, S. Gigan, and M. Cui, *Wavefront shaping for biomedical imaging* (Cambridge University Press, 2019).
11. T. Yeminy and O. Katz, "Guidestar-free image-guided wavefront shaping," Sci. Adv. **7**(21), eabf5364 (2021).
12. J. Bertolotti, E. G. van Putten, C. Blum, A. Lagendijk, W. L. Vos, and A. P. Mosk, "Non-invasive imaging through opaque scattering layers," Nature **491**(7423), 232–234 (2012).
13. O. Katz, P. Heidmann, M. Fink, and S. Gigan, "Non-invasive single-shot imaging through scattering layers and around corners via speckle correlations," Nat. Photonics **8**(10), 784–790 (2014).

Biomedical Optics EXPRESS

14. S. Li, S. A. Horsley, T. Tyc, T. Čižmár, and D. B. Phillips, "Memory effect assisted imaging through multimode optical fibres," Nat. Commun. **12**(1), 1–13 (2021).
15. G. Osnabrugge, R. Horstmeyer, I. N. Papadopoulos, B. Judkewitz, and I. M. Vellekoop, "Generalized optical memory effect," Optica **4**(8), 886–892 (2017).
16. A. M. Paniagua-Díaz, A. Jiménez-Villar, I. Grulkowski, and P. Artal, "Double-pass wavefront shaping for scatter correction in a cataract's model," Opt. Express **29**(25), 42208–42214 (2021).
17. S. Schott, J. Bertolotti, J. F. Léger, L. Bourdieu, and S. Gigan, "Characterization of the angular memory effect of scattered light in biological tissues," Opt. Express **23**(10), 13505–13516 (2015).
18. L. T. Chylack, J. K. Wolfe, D. M. Singer, M. C. Leske, M. A. Bullimore, I. L. Bailey, J. Friend, D. McCarthy, and S. Y. Wu, "The lens opacities classification system III," Arch. Ophthalmol. **111**(6), 831–836 (1993).
19. O. Sahin, A. Pennos, H. Ginis, L. Hervella, E. A. Villegas, B. Cañizares, J. M. Marín, I. Pallikaris, and P. Artal, "Optical measurement of straylight in eyes with cataract," J. Refract. Surg. **32**(12), 846–850 (2016).
20. I. J. van der Meulen, J. Gjertsen, B. Kruijt, J. P. Witmer, A. Rulo, R. O. Schlingemann, and T. J. van den Berg, "Straylight measurements as an indication for cataract surgery," J. Cataract Refractive Surg. **38**(5), 840–848 (2012).
21. T. J. Van Den Berg, "Analysis of intraocular straylight, especially in relation to age," Optom. Vis. Sci. **72**(2), 52–59 (1995).
22. H. Ginis, G. M. Pérez, J. M. Bueno, and P. Artal, "The wide-angle point spread function of the human eye reconstructed by a new optical method," J. Vis. **12**(3), 20 (2012).
23. J. Santamaría, P. Artal, and J. Bescós, "Determination of the point-spread function of human eyes using a hybrid optical–digital method," J. Opt. Soc. Am. A **4**(6), 1109–1114 (1987).
24. H. Ginis, G. M. Perez, J. M. Bueno, A. Pennos, and P. Artal, "Wavelength dependence of the ocular straylight," Invest. Ophthalmol. Visual Sci. **54**(5), 3702–3708 (2013).
25. R. A. Ahmed, K. M. Yoo, R. M. Klapper, and R. R. Alfano, "Time resolved backscattering to monitor different stages of eye cataract," Appl. Opt. **29**(7), 896–897 (1990).
26. Y. Liu, Y. Shen, H. Ruan, F. L. Brodie, T. T. Wong, C. Yang, and L. V. Wang, "Time-reversed ultrasonically encoded optical focusing through highly scattering ex vivo human cataractous lenses," J. Biomed. Opt. **23**(1), 1 (2018).
27. F. A. Bettelheim and A. A. Bettelheim, "Small-angle light scattering studies on xylose cataract formation in bovine lenses," Invest Ophthalmol. Vis. Sci. **17**(9), 896–902 (1978).
28. K. M. Yoo, F. Liu, and R. R. Alfano, "Angle and time-resolved studies of backscattering of light from biological tissues," SPIE. Laser-Tissue Interaction (Vol. 1202, pp. 260–271).
29. A. Paniagua-Diaz, "Optical Memory Effect of excised cataractous human crystalline lenses," Centre for Environmental Data Analysis: Version 1, 28 July 2022, https://doi.org/10.5281/zenodo.6927945.